MODELLING OF NONLINEAR RAIL IMPEDANCE IN AC TRACTION POWER SYSTEMS

Dr R. John Hill Mr David C. Carpenter

University of Bath, School of Electrical Engineering
Claverton Down, Bath BA2 7AY, UK

Abstract - Nonlinearity in the internal self-impedance of railroad rail can give rise to power frequency harmonics in traction systems. Limiting case analytical models of rail impedance, based on linear complex permeability and complete saturation, are compared with measurements for currents to 800A and frequencies to 10 kHz. The results show that for accurate representation an effective permeability of the material must be defined by prior modelling of the eddy current flux distribution within the rail iron. The usual assumption of rail internal self-impedance invariance with current is shown to be unrealistic.

INTRODUCTION

In AC-electrified railways, electric power is delivered from transformer substations via overhead catenary and returned through the running rails to electrical connections with return feeder cables or autotransformers. The traction power transmission system comprises the catenary, auxiliary feeder, return conductor and rail track. Electrically, this forms a coupled multiconductor transmission line, the behaviour of which is described by a matrix equation relating the phase voltages V_i to the line currents I_i, as follows:

$$\frac{d}{dx}[V_i] = [z_{ij}][I_i]. \qquad (1)$$

In this equation, the coefficients of the system impedance matrix are diagonal terms z_{ii}, the self-impedance of each conductor i with earth return, and off-diagonal terms z_{ij}, the mutual impedance between conductors i and j with earth return. The self-impedance terms are the sum of external and internal impedances. The former are functions mainly of circuit geometry, but the latter are determined by the flux within the rail iron. They depend on the excitation current and frequency, and are sources of nonlinearity in the power transmission path.

The elements of the track impedance matrix are required as data for system simulation studies, the objectives of which are to model energy flow, power supply/signal interference and harmonic effects. Harmonic currents generated by rail nonlinearities can propagate back into the power system and couple with communications and track signalling circuits. They can cause power supply problems such as network distortion, line resonance, and power factor deterioration, and are also important for fault condition and transient studies.

In most simulation studies reported in the literature, rail internal self-impedance is treated as an analytic function with value equal to the impedance of an equivalent circular conductor. Rail iron permeability is treated as a constant [1,2], so both resistance and inductance are assumed constant with AC current. The internal inductance reduces and the resistance rises with frequency due to flux reduction and redistribution within the iron from the skin effect. In the steady state, the external self-inductance is usually considered to dominate the internal self-inductance [2], the former being approximated with sufficient accuracy using the Carson-Pollaczek equations assuming the earth to have a finite, constant conductivity. Stanek et al [3], however, show that for transient studies, the rail internal self-impedance may be significant compared with the external component, and that the nature of fault transients indicates that knowledge of its impedance variation with current and frequency is essential for successful modelling of traction fault currents. Significant impedance change occurs from the effects of saturation and hysteresis in the rail iron, both phenomena modifying rail energy losses and reactive power flow. Holmstrom [4] has stated that rail hysteresis may give rise to intermodulation distortion in power and audio frequency track signalling systems.

The problem of the determination of rail self-impedance is concerned with the analysis of power frequency magnetic systems. The literature on this subject has concentrated on modelling saturation and hysteresis effects in electrical machines and transformers by accurate field computational techniques. These applications do not in general deal with magnetic conductors but the analytic methods can still be used with advantage. Burais [5], for example, demonstrates a technique to separate hysteresis from eddy current losses for a non-oriented material steel plate taking into account saturation. The method combines the finite element technique for space, and finite difference for time discretization. A similar problem is approached in a different way by Labridis [6] who assumes an equivalent fictitious material with relative permeability constant in time but variable in space, and related to the saturation B-H curve by a stored magnetic co-energy density. The effect of harmonic fluxes has also been evaluated numerically for transformer cores, and Hsu [7] shows that iron loss can be reduced for saturated conditions where hysteresis loss is large.

The modelling of internal impedance in an irregular-shaped ferromagnetic conductor such as railroad rail suffers practical difficulties due to its shape and variable material permeability. In this paper, the objectives of the modelling of rail internal impedance are to determine the regimes where hysteresis and saturation effects are significant. Linear analytic models with actual material data based on measurements of rail material permeability and resistivity are presented. The rail internal self-impedance term in the track impedance matrix is evaluated as a function of both frequency and AC current. The result can then be used to give a quantitative assessment of the extent of power frequency harmonic propagation in the power delivery process.

0885-8977/91$01.00©1991 IEEE

RAIL MATERIAL DATA

The Ferromagnetic B-H Loop

The permeability (μ) of ferromagnetic material is a function of the field vectors **B** (magnetic induction), **M** (magnetic polarization), and **H** (magnetic field), according to

$$\mathbf{B} = \mu_0(\mathbf{H} + \mathbf{M}) = \mu\mathbf{H} \qquad (2)$$

For isotropic and homogenous materials, the permeability is invariant with direction and position. For ferromagnetic materials, the magnetization process is time-dependent and **B** is a nonlinear, multivalued function of **H** as well as a function of frequency, with

$$\mathbf{B} = \mu(\mathbf{H}, \mathbf{B}, \omega)\,\mathbf{H} \qquad (3)$$

To determine the flux distribution within these materials, and hence electrical impedance, the complete B-H relationship needs to be specified. Figure 1 shows a typical ferromagnetic material static B-H characteristic together with the associated permeability definitions. Of principal interest for large-signal AC conditions are the initial, normal, incremental and differential permeabilities.

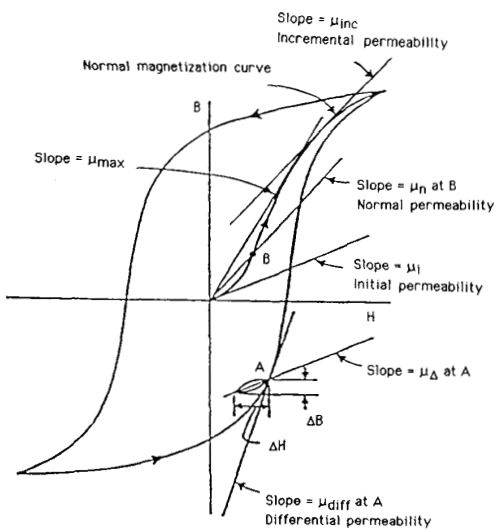

Fig. 1. Ferromagnetic material B-H loop and permeability definitions.

Time dependency in the magnetization process may be accounted for by introducing a complex permeability to describe the phase lag between the **H** and **B** vectors. Thus

$$\mathbf{B}\,e^{j\omega t} = |\mu^*|\,\mathbf{H}\,e^{j(\omega t-\phi)} = (\mu' - j\mu'')\,\mathbf{H}e^{j\omega t} \qquad (4)$$

where μ^* is the complex permeability. Physically, the phase angle accounts for energy losses associated with magnetic resonance and relaxation phenomena arising from the reorientation of magnetic moments of microscopic origin [8]. However a similar representation can also give accurate estimates of material behaviour in the macroscopic region if there is no material saturation, so that the vectors **B** and **H** are linearly related. The B-H characteristic then becomes elliptical. Even for practical materials with nonlinear permeability, approximating the B-H loop by an ellipse allows complex permeability data to be extracted by considering the fundamental frequency relationship.

Experimental Material Tests

Various material samples were machined from railroad rail in order to evaluate the actual permeabilities as specified in Figure 1. The static B-H loop was determined using filaments of material 2 mm square and with length at least 100 mm. Each filament was subjected to an alternating magnetic field with frequency 0.33 Hz in the direction of its longitudinal axis. This low excitation frequency ensured that the skin depth was much greater than the filament width (d):

$$\delta = \sqrt{(2/\omega\sigma\mu)} \gg d \qquad (5)$$

Three filaments from orthogonal directions were tested to confirm the material isotrophy. Graphical results for low, medium and high values of surface field strength H_S are shown in Figure 2. Table 1 shows the evaluated energy per cycle in each of the three hysteresis loops. The variations of normal and incremental permeability as a function of surface magnetic field strength, extracted from the measured data of Figure 2, are reproduced in Figure 3.

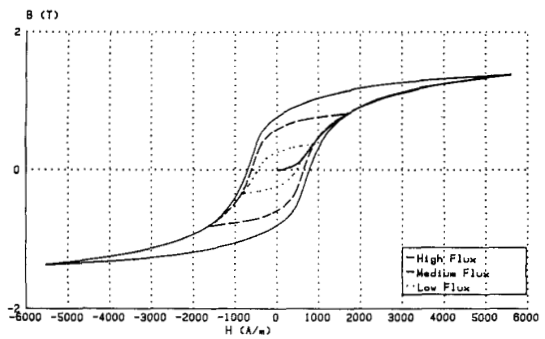

Fig. 2. Measured B-H loops for 54 kg/m flat-bottom rail material.

From the B-H loops, complex permeability data has been evaluated in two ways:

- Assuming sinusoidal magnetic field excitation, the B-H loop has been analysed by the Fast Fourier Transform technique to obtain the fundamental and harmonic magnitudes and phases of the flux density. Only the odd harmonics are significant, and the results for the first three are shown in Table 1. In this method, the sum of the fundamental and harmonic losses will equal the total loss as given by the loop area.
- For linear modelling it may be more accurate to equate the total loop area with the area of an equivalent fundamental ellipse. Thus all harmonic losses would be included within the fundamental. The orientation of the ellipse, defined by coercive force and remanent flux density, is that defined by the original hysteresis loop.

Figure 4 shows the resulting complex permeability functions derived from each model.

Rail Resistivity

The resistivity of the rail iron is also a fundamental material property and appears as a constant in the skin depth function. It can be expressed in the form

$$\rho = \rho_{20}(1 + \alpha T) \qquad (6)$$

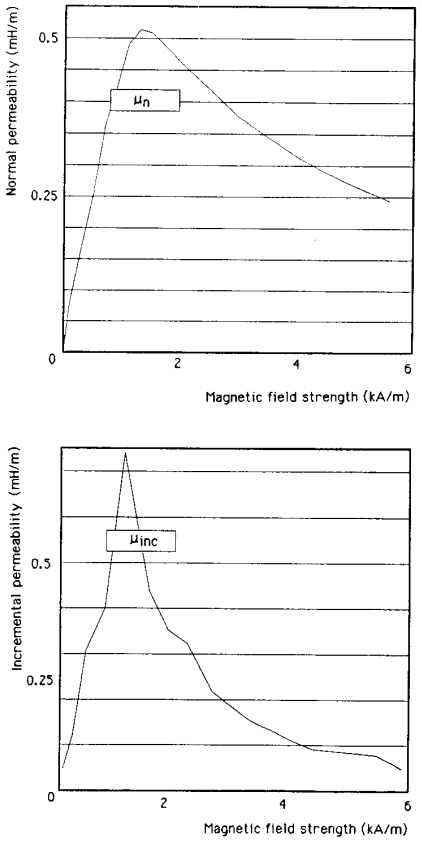

Fig. 3. Derived normal and incremental permeabilities for 54 kg/m rail material.

where α is the temperature coefficient of resistivity, linearized over the temperature range of interest, T is the temperature (K), and ρ_{20} is the restivity at 20 K.

The resistivity of the rail samples used in the material tests was measured by applying constant currents and measuring voltage over a suitable temperature range. Typical results at 20 K are

$$\alpha = 3.4\ 10^{-3}\ K^{-1}$$
$$\rho_{20} = 0.225\ 10^{-6}\ \Omega\ m$$

with conductivity

$$\sigma_{20} = 4.44\ 10^{6}\ S\ m^{-1}.$$

ANALYTICAL MODELLING

The objective of analytical modelling is to predict the dependency of rail internal self-impedance on AC current and frequency. Simple modelling can reveal order of magnitude estimates for the fundamental and harmonic power loss for the base cases of:

- Linear complex permeability, no saturation.
- No hysteresis loss, high saturation.

Further analysis is necessary to establish the optimum effective permeability to use in each model, as a function of surface magnetic field H_s.

Peak surface magnetic field H_s (A m^{-1})	Fundamental B_1 (T)	Φ_1 (°)	3rd harmonic B_3 (T)	Φ_3 (°)	5th harmonic B_5 (T)	Φ_3 (°)	7th harmonic B_7 (T)	Φ_7 (°)
5600	1.65	-9	0.39	-29	0.19	-46	0.105	-65
1700	0.95	-25	0.19	-74	0.075	+65	0.04	+20.5
900	0.394	-26	0.065	+64	0.017	-20	0.006	-73

Table 1. Flat-bottom Rail Hysteresis Loop Harmonic Analysis.

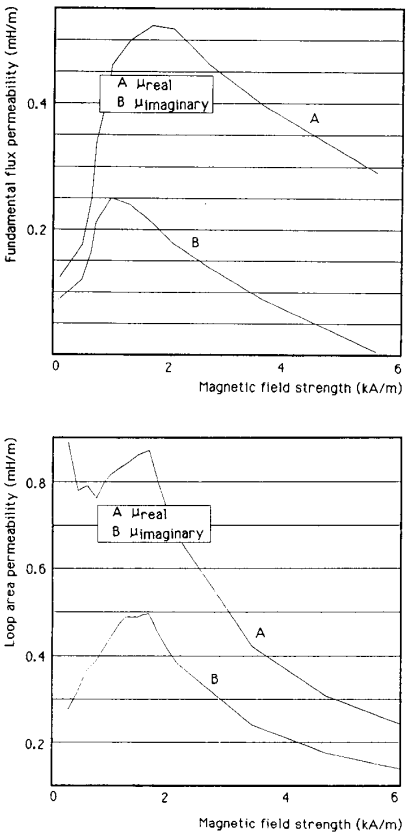

Fig. 4. Complex permeability with fundamental flux and B-H loop area approximations.

Linear Hysteresis Model

The rail is treated as a magnetic conductor made from homogenous, isotropic material with constant permeability μ^*. Assuming an equivalent circular solid conductor, the solution for magnetic field and hence current density within the material is found from solving the diffusion equation [9]. The conductor impedance is then found as a function of conductor radius and skin depth:

$$R + jX = \frac{\alpha}{2\pi a\sigma} \frac{I_0(\alpha a)}{I_1(\alpha a)} \qquad (7)$$

where

$$\alpha^2 = j\omega\sigma\mu^* \qquad (8)$$

is the complex skin depth function, a is the conductor

radius, σ is the conductivity and I_n are n^{th} order modified Bessel functions of the first kind.

After manipulation, it may be shown that the internal impedance of the conductor takes limiting values at low and high frequencies as follows [10]:

Low frequency: $a \ll \delta$

$$z_{lf} = \frac{1}{\pi a^2 \sigma}\left\{\left[1 + \frac{a^2}{4\delta^2}\sin\theta + \frac{a^4}{48\delta^2}\cos 2\theta\right] + j\left[\frac{a^2}{4\delta^2}\cos\theta - \frac{a^4}{48\delta^4}\sin 2\theta\right]\right\} \quad (9)$$

High frequency: $a \gg \delta$

$$z_{hf} = \frac{1}{\pi a^2 \sigma}\left\{\left[\frac{1}{4} + \sqrt{2}\cos\left(\frac{\pi}{4} - \frac{\theta}{2}\right)\right]\left(\frac{a}{2\delta} + \frac{3}{32}\frac{\delta}{a}\right) + j\left[\sqrt{2}\sin\left(\frac{\pi}{4} - \frac{\theta}{2}\right)\right]\left(\frac{a}{2\delta} - \frac{3}{32}\frac{\delta}{a}\right)\right\} \quad (10)$$

where θ is the hysteresis angle. For complex permeability, Equations (9) and (10) describe the behaviour at the fundamental frequency, and the eddy and hysteresis losses cannot be separately identified.

The impedance angle reduces with hysteresis from the asymptotic value of π/4. The model shows that losses are increased in the presence of hysteresis by a factor

$$\frac{[\cos(\pi/4 - \theta/2)]}{\cos\pi/4}$$

and the rail reactance is decreased by the factor

$$\frac{[\sin(\pi/4 - \theta/2)]}{\sin\pi/4}.$$

Saturation Effects

The linear model gives the equivalent rail impedance as that of an inductance, associated with energy storage, and a resistance, associated with energy dissipation. In electrical circuits, a nonlinear resistance behaves like a reactive power generator, although it has no energy-storage capacity. This is also the case for a saturated magnetic system, where the nonlinearity modifies the reactive, as well as the active power. An approximate model to take account of saturation in rail can represent the iron B-H characteristic by a step function according to

$$B = \begin{cases} +B_A & H > 0 \\ -B_A & H < 0 \end{cases} \quad (11)$$

It can be shown [9] that for this material property, magnetic flux waves with a constant magnitude of $|B_A|$ will penetrate the boundary under the influence of sinusoidal surface magnetic field excitation ($H_S \sin \omega t$). The maximum penetration depth is:

$$\delta_A = \sqrt{[2H_S/\omega\sigma B_A]} \quad (12)$$

which is in the same form as the skin depth equation (5), with the effective permeability, μ, replaced by B_A/H_S. The average power in the material is

$$P_{av} = \frac{8}{3\pi}\frac{H_S^2}{\sigma\delta_A} \quad (13)$$

which is a factor 70% greater than that in the linear case (with δ set equal to δ_A).

Eddy Current Loss Model

The approximate models described so far represent limiting conditions of linear permeability and complete saturation. In most cases, the rail material saturates gradually, accompanied by distortion in the hysteresis loop. The balance between hysteresis and eddy current losses then changes.

The effect of nonlinear permeability in the presence of hysteresis is to produce harmonics with associated extra losses. To predict the rail impedance variation under these conditions a suitable effective permeability value must be selected. The modified eddy current distribution within the material can be calculated numerically taking account of the known dependency of permeability on magnetic field strength. The approach adopted is to use a finite difference technique, the Du Fort-Frankel scheme [11], to calculate the spatial and temporal decay in the magnetic field intensity within the material and hence estimate the effective complex skin depth.

The finite difference technique gives an explicit equation with attractive stability properties. Applied to a semi-infinite slab of material, the magnetic field strength is given by

$$\frac{\partial^2 H}{\partial y^2} = \sigma\mu(H)\frac{\partial H}{\partial t} \quad (14)$$

The associated difference equation is:

$$H_{i,k+1} = r H_{i+1,k} + (1-2r) H_{i,k} + r H_{i-1,k} \quad (15)$$

where $r = p/\sigma\mu h^2$, p being the time step length and h the spatial step length. By substituting for the present nodal value the average of the previous and next values,

$$H_{i,k} = (H_{i,k+1} + H_{i,k-1})/2 \quad (16)$$

the explicit difference equation is formed:

$$H_{i,k+1} = H_{i,k-1} + \frac{2r}{2r+1}(H_{i+1,k} - 2H_{i,k-1} + H_{i-1,k}). \quad (17)$$

The distribution of H in the material can then be determined by varying the surface magnetic field strength $H_{0,k}$ as a sine wave. Figure 5 shows the computed result of $|H_S|$ vs depth, for various initial surface field strengths. At high field strengths, the material becomes saturated near the surface and the magnitude of H falls away steeply in the interior, but for low initial field strengths, there is little deviation from the linear model.

EXPERIMENTAL RAIL IMPEDANCE MEASUREMENTS

Order of Magnitude Estimate for Hysteresis and Eddy Losses

In order to determine the relative importance of hysteresis and eddy current losses, iron losses were measured as a function of frequency in a toroid manufactured from rail iron. The dimensions of the toroid were: radius 30 mm, thickness 3 mm and length 10 mm, and the winding comprised 250 turns of 1 mm copper wire. The results, shown in Figure 6 with the static B-H loop loss per cycle superimposed, show that at power frequencies the hysteresis loss and eddy loss per cycle are comparable. This indicates that for the range of rail excitation expected in practice, neither the linear nor the heavily saturated model alone is realistic.

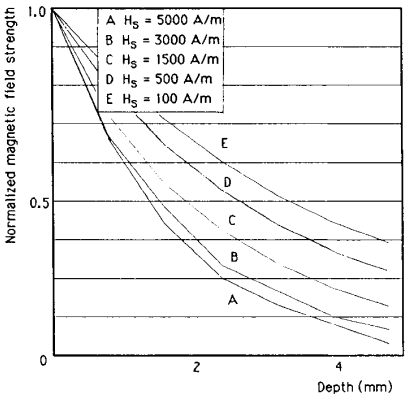

Fig. 5. Magnetic field strength as a function of depth in a semi-infinite slab of ferromagnetic material.

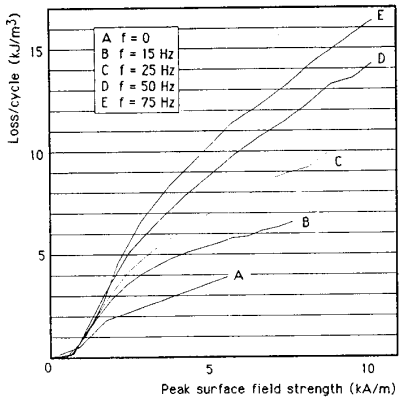

Fig. 6. Measured iron loss in toroid sample of rail material.

Rail Impedance Measurement Apparatus

To accurately measure the rail internal self-impedance, the circuit inductance due to the test current return path and the flux disturbance from sample shape effects must both be eliminated. The experimental technique used was developed from equipment described by Holmstrom [4] for null-flux measurement of the self-inductance change in an isolated rail, using as a reference conductor a copper tube. The method was modified so that absolute measurements of internal impedance could be made. The apparatus (Figure 7) relies on the prior use of a reference conductor, which is a specially-constructed hollow copper shell of identical shape to the test rail and having negligible internal inductance [10] at high frequency. This enables the impedance measurement loop to be adjusted in position (distance d in Figure 7) such that zero inductance is obtained in calibration.

When the rail sample is placed in the same physical position as the copper shell, measurements of the change in inductance will thus represent the true internal self-inductance. The resistive part of the impedance remains an absolute measurement of internal resistance. End effects are negligible since the measurement points (A, B in Figure 7) are maintained a suitable distance from the conductor ends. An on-line FFT analyser provides noise immunity and accurate phase and frequency measurement.

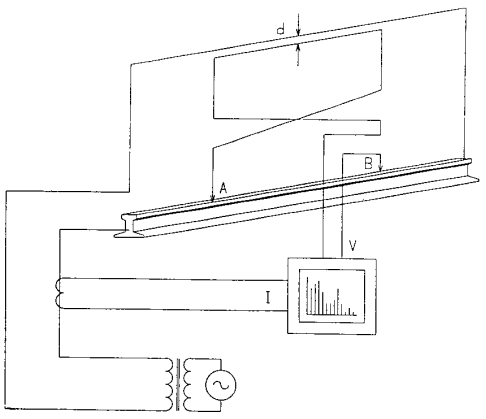

Fig. 7. Experimental apparatus for measurement of rail impedance.

Rail Impedance as Function of Current and Frequency

Measurement results of impedance as a function of current at 50 Hz are shown in Figure 8. Both resistance and inductance increase with current magnitude for the range of currents generated. To assess rail impedance at harmonic frequencies, measurements at a constant amplitude of 6 A were made for frequencies up to 10 kHz. The results are shown in Figure 9. As expected, the resistance increases and the inductance decreases with increasing frequency due to the skin effect.

DISCUSSION

Superimposed on the experimental curves of Figures 8 and 9 are theoretical calculations derived from the various assumptions on the modelling of hysteresis loss and the variation in material permeability. The increase of rail impedance with AC current indicates that the material is far from saturation even with the highest current applied. This is because of the large rail cross sectional area ($7.5\ 10^{-3}$ m^2). The most accurate resistance model is with an effective permeability function at low excitation, and with complex permeability obtained by the B-H loop area approximation (i.e. incorporating total harmonic losses within the fundamental) at high excitation. The use of normal and incremental permeability from Figure 3 is inappropriate in the model due to the importance of hysteresis loss. The effective permeability used is constant throughout the AC cycle, but with magnitude dependent on the level of current excitation as determined from Figure 5 (it has been termed *linearized* permeability). The inductance variation shows good agreement with the model using complex permeability obtained from the fundamental of the B-H loop, with better agreement at very low excitations from the linearized model of permeability as described above.

The variation in rail resistance with frequency, for low excitation currents, shows good agreement with the complex permeability model based on total loop area for high frequencies, and that based on the fundamental component for low frequencies. For rail inductance, the fundamental complex permeability model is more accurate at high frequencies, with the experimental curve lying between this model and the linearized model of permeability at lower frequencies.

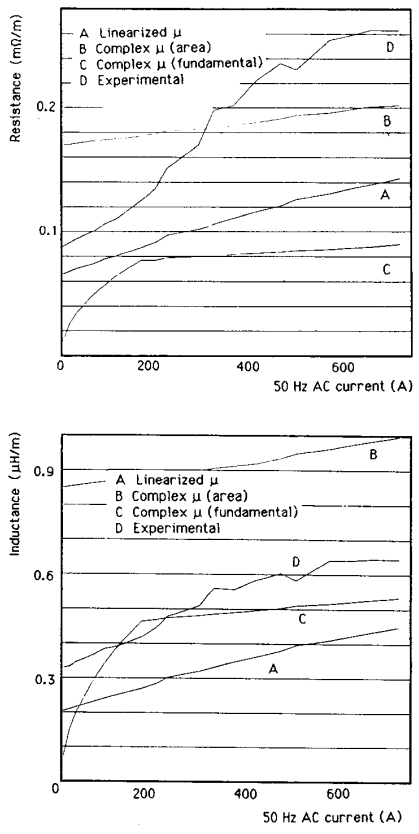

Fig. 8. Experimental and theoretical rail internal self-impedance as a function of AC current at 50 Hz.

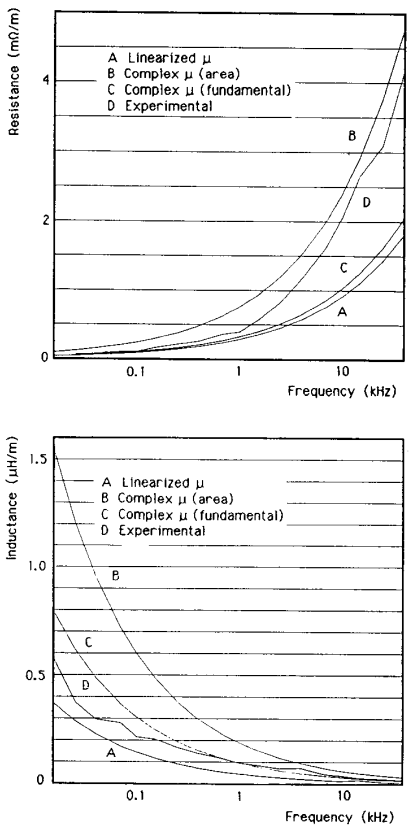

Fig. 9. Experimental and theoretical rail internal self-impedance as a function of frequency at 6A.

The complex permeability model based on loop area is more accurate for rail resistance modelling at high currents and frequencies. This model necessarily includes higher harmonic losses which increase with greater excitation. For the rail induction variation with current, ignoring the harmonics produces closer agreement with the experimental measurements. However the inductance is defined only at the fundamental frequency and the total VARs would necessarily need to include higher harmonics.

More accurate models are required to represent the rail impedance over the complete range of current and frequency. For example, accurate computations using combined finite element and finite difference techniques could incorporate exact differential permeability data, and hence enable identification of the separate fundamental and harmonic losses.

CONCLUSIONS

An analytical model with linear complex permeability, based on experimental determination of the material B-H loop, gives good agreement with measurements of rail impedance for moderate rail currents. The conditions correspond to hysteresis but not saturation, and will be of use in the modelling of power harmonic propagation in track signalling systems. At low excitations, better agreement is found by neglecting hysteresis and using an effective permeability obtained by modelling the flux distribution within the rail, using as data experimentally derived normal permeability as a function of surface magnetic field strength.

A saturation model ignoring hysteresis is suggested as suitable for transient studies and fault condition analyses which would be obtained with high excitation currents. The large magnitude of current at 50 Hz necessary to achieve rail saturation was not achieved in the reported experiments.

Results presented for rail internal self-impedance will enable the rail resistance and inductance at specific power frequency harmonics to be determined. The impedance is a function of current and frequency and cannot be obtained as a closed-form expression. It could, however, be expressed as a polynomial.

ACKNOWLEDGEMENTS

This research was supported by the Science and Engineering Research Council, UK.

REFERENCES

[1] D. J. Tylavsky and A. Y. Kulkarmi, "Inductance calculations for earth-return trolley systems," Proceedings of *1988 IEEE Industry Applications Society Annual Meeting*, Pittsburgh PA, 2-7 October 1988 (New York: IEEE 1988), vol. 2, pp. 1216-1223.

[2] B. Mellitt, J. Allan, Z. Y. Shao, W. B. Johnston and C. J.

Goodman, "Computer-based methods for induced-voltage calculations in AC railways," *IEE Proceedings,* vol. 137B, no. 1, pp. 59-72, January 1990.

[3] E. K. Stanek, T. Cataltepe and D. O. Wiitanen, "Phenomena that affect the calculation of the inductance and resistance of mine track/trolley systems," Proceedings of *1984 IEEE Industry Applications Society Annual Meeting,* Chicago IL, 30 September - 4 October 1984 (New York: IEEE 1984), pp. 100-106.

[4] F. R. Holmstrom, "The model of conductive interference in rapid transit signaling systems," *IEEE Transactions on Industry Applications,* vol. IA-22, no. 4, pp. 756-762, July/August 1986.

[5] N. Burais and G. Grellet, "Numerical modelling of iron losses in ferromagnetic steel plate," *IEEE Transactions on Magnetics,* vol. MAG-18, no. 2, pp. 558-61, March 1982.

[6] D. Labridis and P. Dokopoulos, "Calculation of eddy current losses in nonlinear ferromagnetic materials," *IEEE Transactions on Magnetics,* vol. MAG-25, no. 3, pp. 2665-2669, May 1989.

[7] J. S. Hsu, H. H. Woodson and S.-S. P. Liou, "Experimental study of harmonic-flux effects in ferromagnetic materials," *IEEE Transactions on Magnetics,* vol. MAG-25, no. 3, pp. 2678-2685, May 1989.

[8] D. J. Epstein, "Permeability". In: *Dielectric Materials and Applications* [Editor: A. R. Von Hippel]. New York: Technology Press M.I.T./Wiley 1954.

[9] P. Hammond. *Applied Electromagnetism.* Oxford UK: Pergamon Press 1981.

[10] D. C. Carpenter and R. J. Hill, "The effect of magnetic saturation, hysteresis and eddy currents on rail track impedance," Proceedings of *IEEE/ASME Joint Railroad Conference,* Philadelphia PA, 25-27 April 1989 (New York: IEEE 1989), pp. 73-79.

[11] E. C. Du Fort and S. P. Frankel, "Stability conditions in numerical treatment of parabolic differential equations," *Mathematical Tables and Aids Computation,* vol. 7, pp. 135-152, 1953.

R. John Hill was born in Somerset, England, on July 3, 1948. He received the degrees of B.Eng. in Electronics and Ph.D. in Power Electrical Engineering from the University of Liverpool, England, in 1969 and 1973, and M.A. from the University of Cambridge, England, in 1983.

From 1973-1980 he was a Design and Development Engineer for London Underground Railways working on automatic train control systems. In 1980 he became a Lecturer at Cambridge University Engineering Department and in 1983 a Fellow of King's College, Cambridge. Since 1986 he has been a Lecturer at the Universaity of Bath, England.

Dr Hill is a Member of the IEE (UK) and the Institute of Physics (UK). In 1988 he was awarded the IEEE Vehicular Technology Society prize for the best paper presented at the Joint ASME/IEEE Railroad Conference.

David C. Carpenter was born in England on September 8, 1956. He received the degrees of B.Sc. from the University of Southampton, England, in 1978 and M.Phil. from Coventry Polytechnic, England, in 1989.

In 1979 he became a Computer-Aided Design Engineer at GEC Machines Ltd, Rugby, England, and in 1980 a Lecturer (Senior Lecturer from 1984) in Electrical Engineering at Coventry Polytechnic, England. From 1986-1987 he was a Visiting Professor at Lakehead University, Canada. Since 1988 he has been a Research Officer at the University of Bath, UK, working on the modelling of electric traction systems.

Mr Carpenter is a Member of the IEE (UK).